



Supporting Information

for *Small*, DOI: 10.1002/smll.202200847

Anomalous Structural Evolution and Glassy Lattice in Mixed-Halide Hybrid Perovskites

*Shamim Shahrokhi, Milos Dubajic, Zhi-Zhan Dai, Saroj Bhattacharyya, Richard A. Mole, Kirrily C. Rule, Mohan Bhadbhade, Ruoming Tian, Nursultan Mussakhanuly, Xinwei Guan, Yuewei Yin, Michael P. Nielsen, Long Hu, Chun-Ho Lin, Shery L. Y. Chang, Danyang Wang, Irina V. Kabakova, Gavin Conibeer, Stephen Bremner, Xiao-Guang Li, Claudio Cazorla, and Tom Wu**

Supporting Information

Anomalous Structural Evolution and Glass Lattice Behaviour in Mixed-Halide Hybrid Perovskites

Shamim Shahrokhi^{1,#}, Milos Dubajic^{2,#}, Zhi-Zhan Dai³, Saroj Bhattacharyya⁴, Richard A. Mole⁶, Kirrily C. Rule⁶, Mohan Bhadbhade⁴, Ruoming Tian⁴, Nursultan Mussakhanuly², Xinwei Guan¹, Yuewei Yin³, Michael P. Nielsen², Long Hu¹, Chun-Ho Lin¹, Shery L. Y. Chang^{1,5}, Danyang Wang¹, Irina V. Kabakova⁷, Gavin Conibeer², Stephen Bremner², Xiao-Guang Li³, Claudio Cazorla^{8,*}, Tom Wu^{1,*}

#authors with equal contribution

*Corresponding author, Email: claudio.cazorla@upc.edu, tom.wu@unsw.edu.au

Section 1. Thermal Properties

Table S1. Temperatures, Enthalpies and Entropies of the Phase Transitions of MAPbI₃ and MAPbBr₃.

	T_{trs} (K)	ΔH (kJ.mol ⁻¹)	ΔS (J.mol ⁻¹ .K ⁻¹)
MAPbI ₃	165	2.36	14.33
	331	0.22	0.66
MAPbBr ₃	151	1.37	9.07
	156	0.30	1.92
	236	0.14	0.59

Section 2. Structural Characterizations

Supplemental Text

Single-Crystal X-ray Diffraction Analysis

SCXRD measurements were performed on mixed-halide single crystals at 300 K and 100 K to determine the crystal structures. At 300 K, the structure is mostly dominated by monoclinic (pseudocubic) with the diffraction patterns including major spots^[1] (**Figure S2a,c**). By decreasing the temperature down to 100 K (**Figure S2b,d**), some low intensity points appeared in between the main Bragg peaks, indicating the existence of the orthorhombic structure, which is consistent with simulated SCXRD patterns.^[2-3] However, slight differences in the number of spots between experimental and simulated patterns represent possible co-existence of cubic, tetragonal and orthorhombic structures beside monoclinic as the dominant phase at lower temperatures (**Figure S3**).

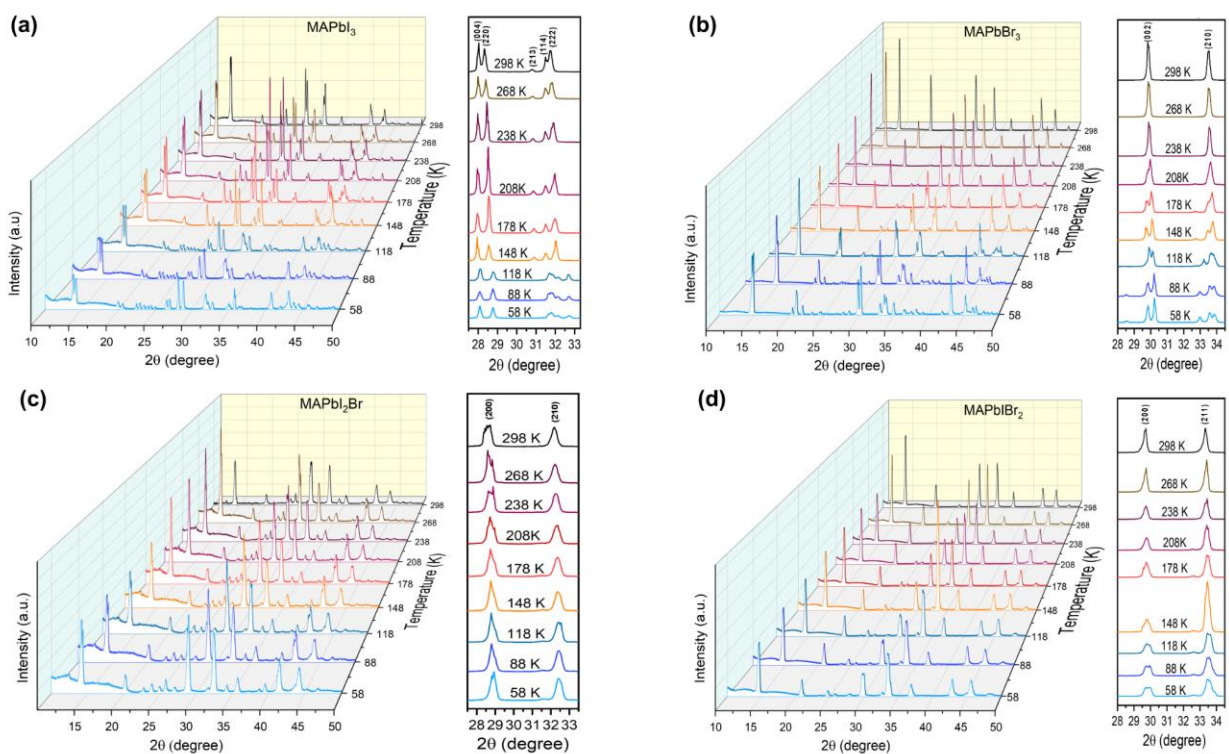
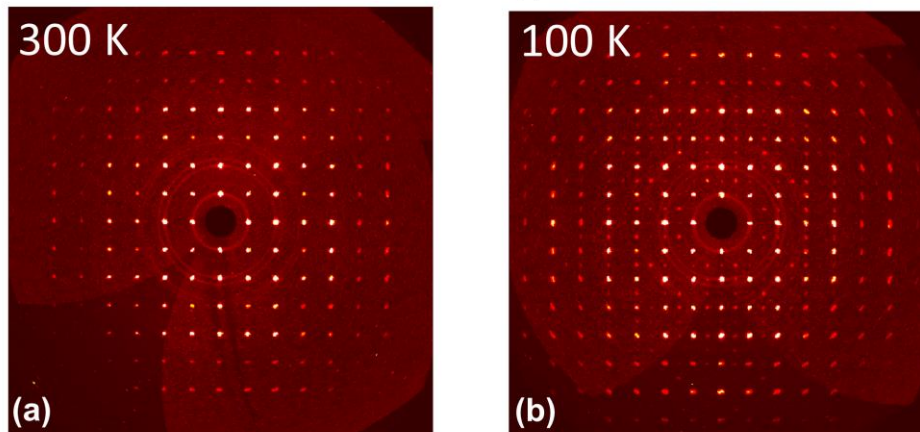


Figure S1. VT-PXRD patterns of a) MAPbI_3 , b) MAPbBr_3 , c) MAPbI_2Br and d) MAPbBr_2 single crystals at different temperatures ($\lambda = 1.5406 \text{ \AA}$). The splitting of peaks corresponding to phase transitions are evident in selected diffraction lines for pure hybrid halide perovskites.

MAPbI₂Br



MAPbIBr₂

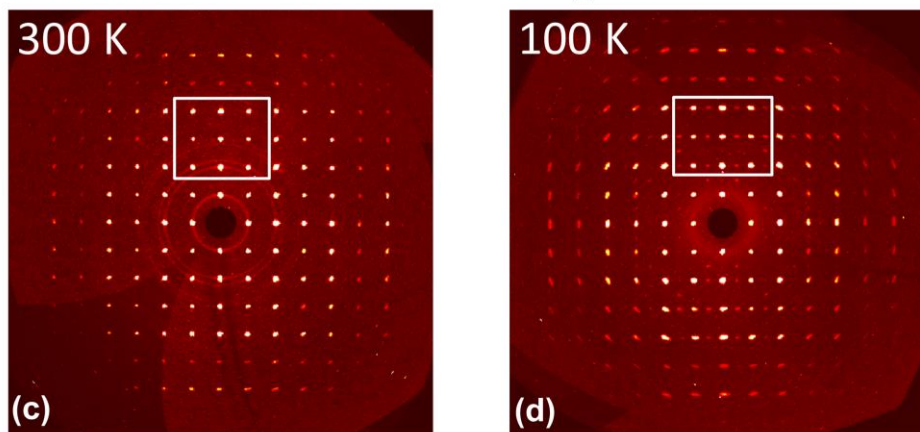
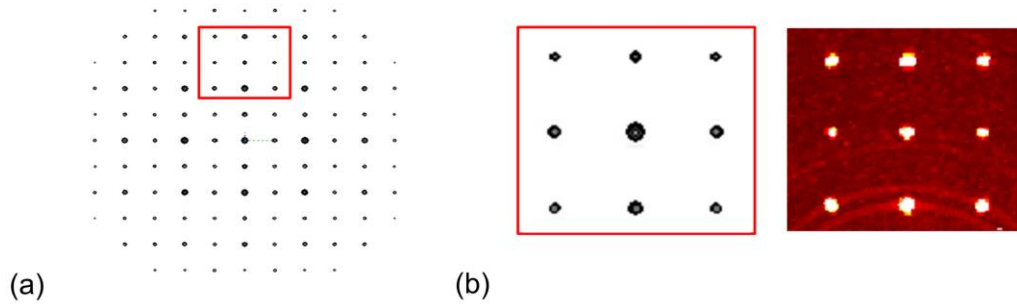


Figure S2. Reciprocal lattice reconstructions of MAPbI₂Br and MAPbIBr₂ single crystals at a,c) 300 K, and b,d) 100 K from (0kl) plane. The white squares are related to magnified regions in simulated patterns of Figure S3.

MAPbIBr₂

Monoclinic



Orthorhombic

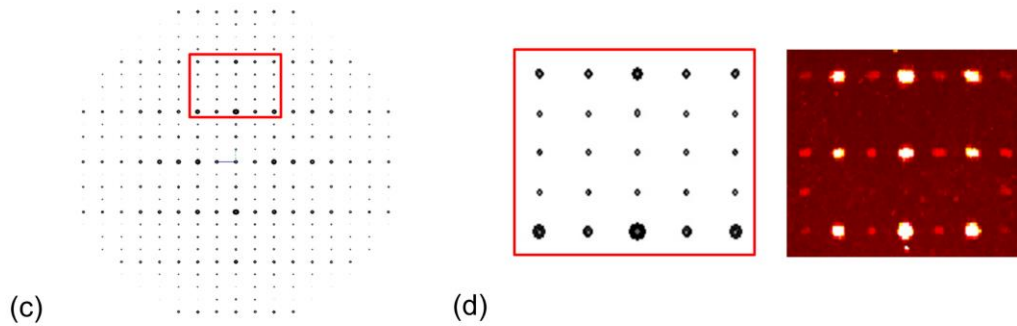


Figure S3. Simulated reciprocal space reconstructions of MAPbIBr₂ single crystal from (0kl) plane in a) monoclinic and c) orthorhombic structures. The magnified simulated and corresponding experimental patterns of the regions in red squares of monoclinic and orthorhombic images are presented in b,d), respectively. The relative intensity distributions between the major and weak spots and the periodic changes of intensity ratios demonstrate the difference in structures.

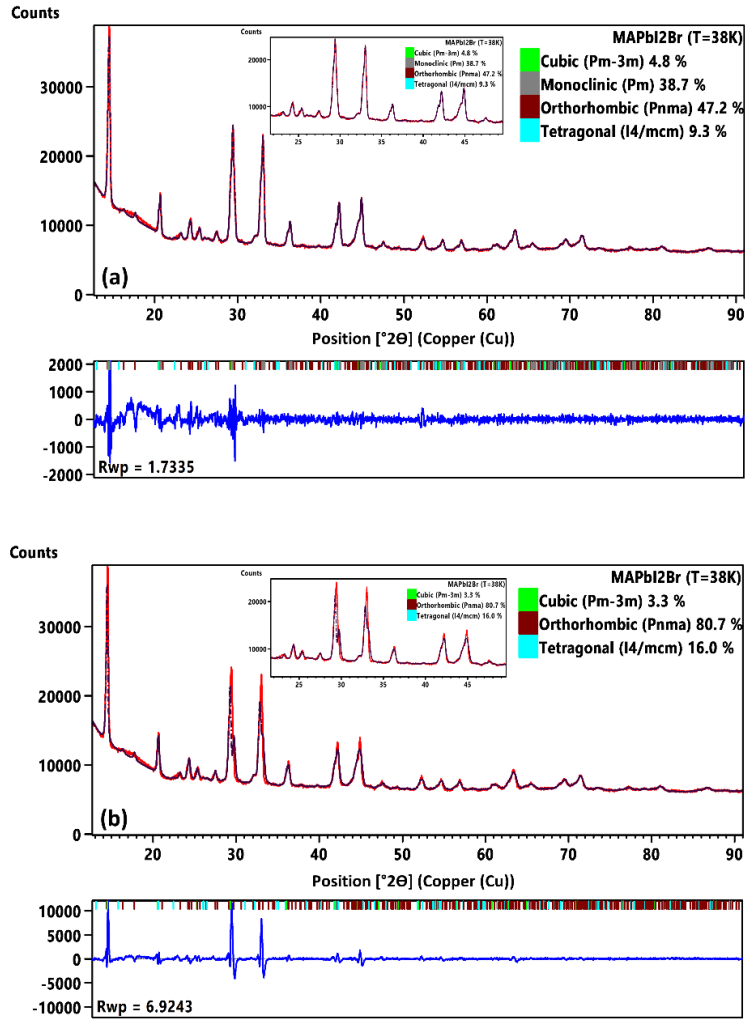


Figure S4. Pawley refinements from PXRD patterns of MAPbI₂Br a) with and b) without monoclinic structure at 38 K. The black dots, red and blue lines and the bars correspond to calculated intensity, experimental intensity, difference between calculated and experimental intensity plots and Bragg positions, respectively. The refinements including monoclinic structure represent lower R_{wp}.

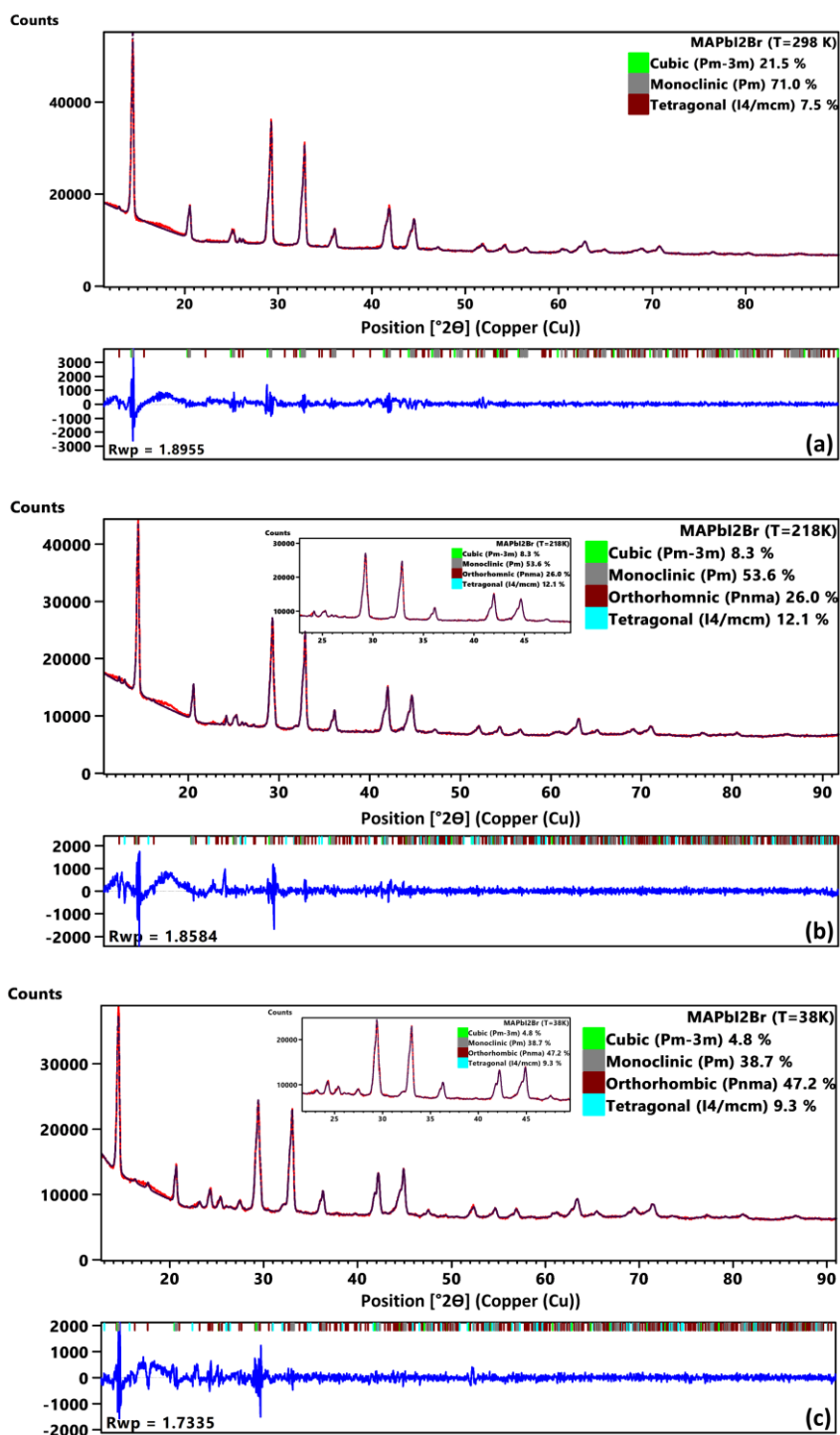


Figure S5. Pawley refinements from PXR patterns of MAPbI₂Br at a) 298 K, b) 218 K and c) 38 K. The black dots, red and blue lines and the bars correspond to calculated intensity, experimental intensity, difference between calculated and experimental intensity plots and Bragg positions, respectively.

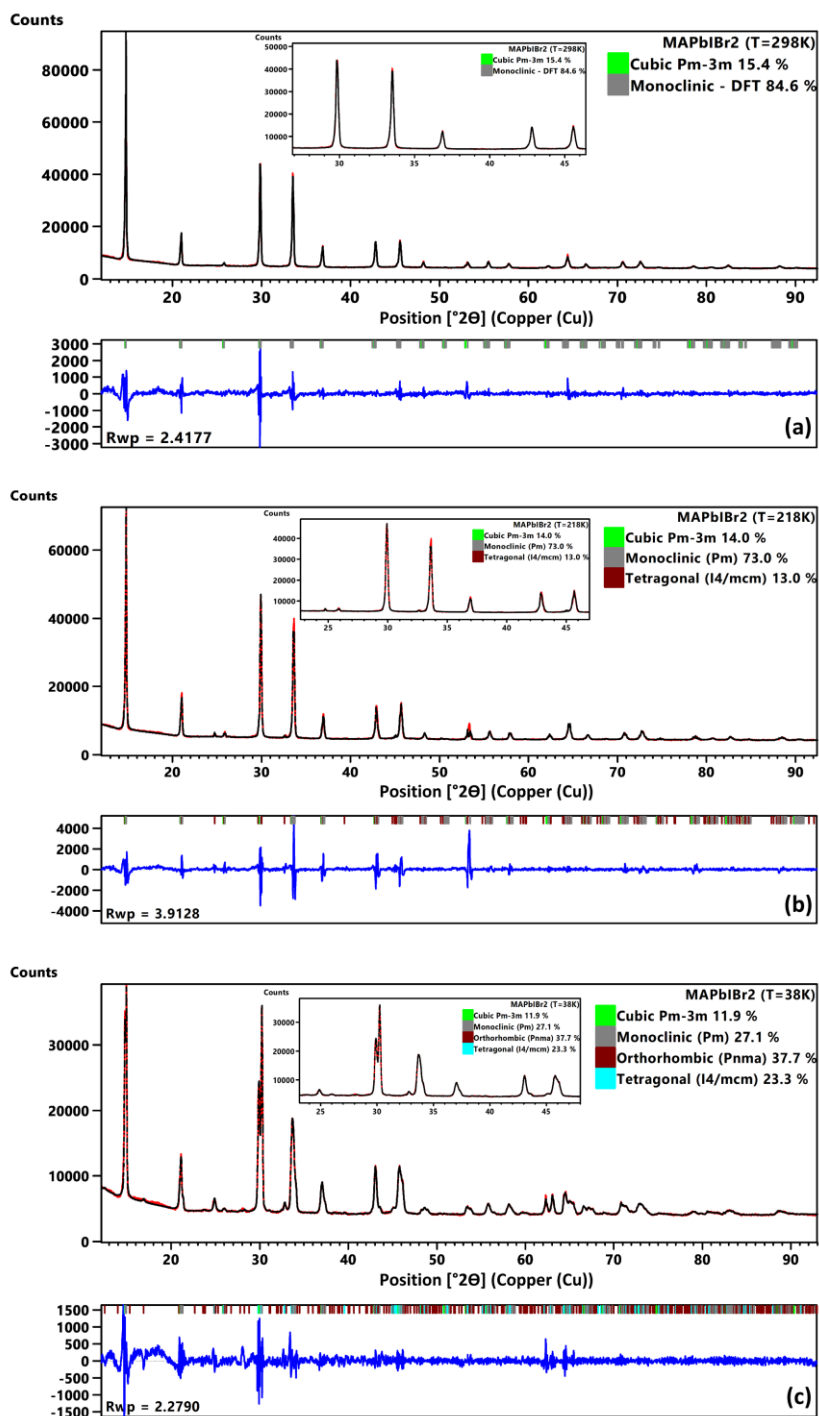


Figure S6. Pawley refinements from PXRD patterns of MAPbI₂Br₂ at a) 298 K, b) 218 K and c) 38 K. The black dots, red and blue lines and the bars correspond to calculated intensity, experimental intensity, difference between calculated and experimental intensity plots and Bragg positions, respectively.

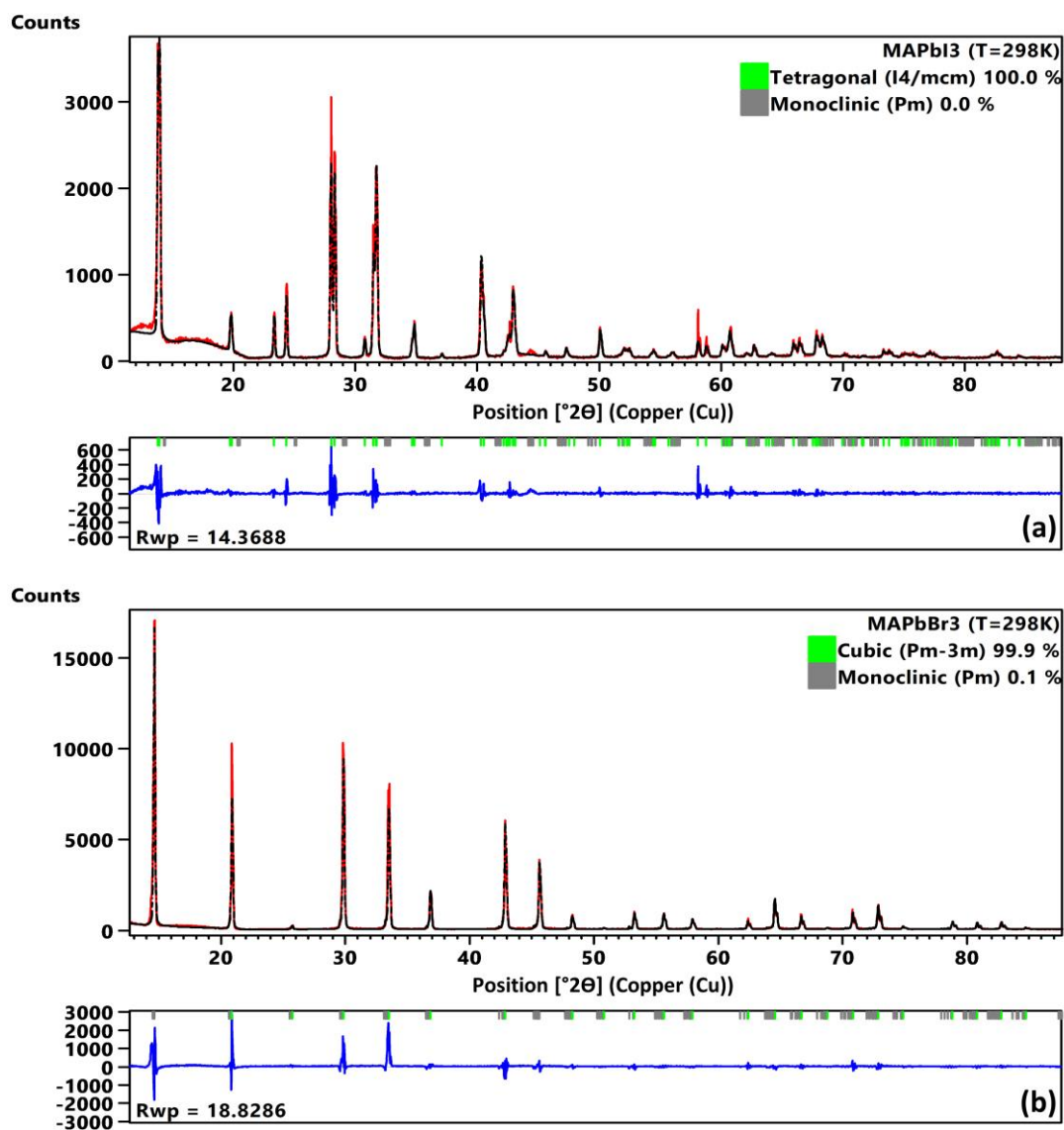


Figure S7. Rietveld refinements from PXRD patterns of a) MAPbI₃ and b) MAPbBr₃ at room temperature. The black dots, red and blue lines and the bars correspond to calculated intensity, experimental intensity, difference between calculated and experimental intensity plots and Bragg positions, respectively.

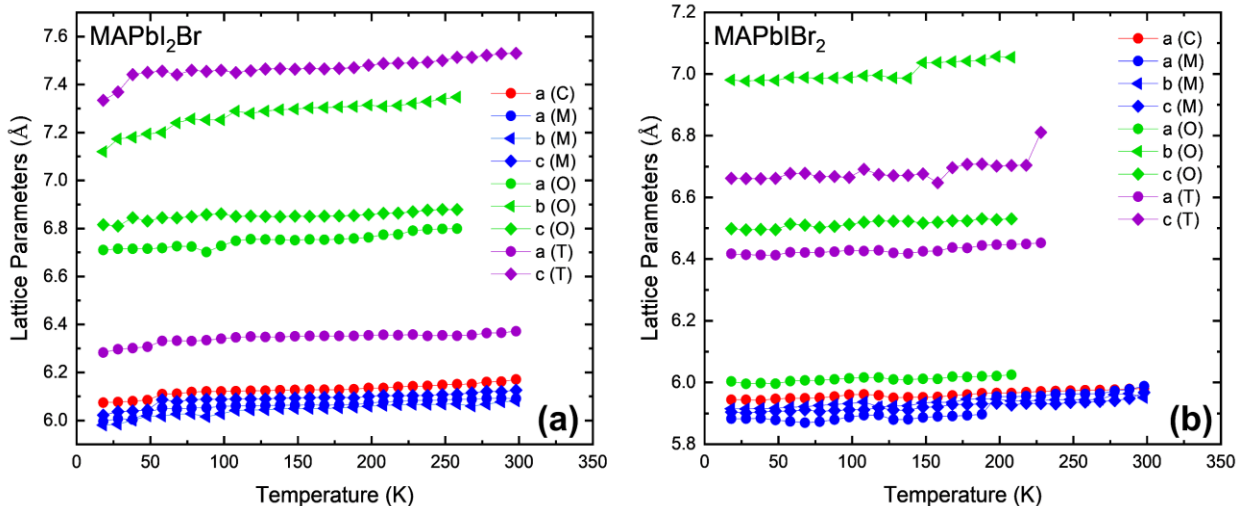


Figure S8. Lattice parameters of a) MAPbI₂Br and b) MAPbIBr₂ calculated from fitting to the PXRD patterns. Besides the cubic (space group: *P-43m*), orthorhombic (*Pnma*), and tetragonal (*I4/mcm*) phases previously reported for halide perovskites, a hitherto unreported monoclinic (*Pm*) phase with slight lattice distortion was discovered.

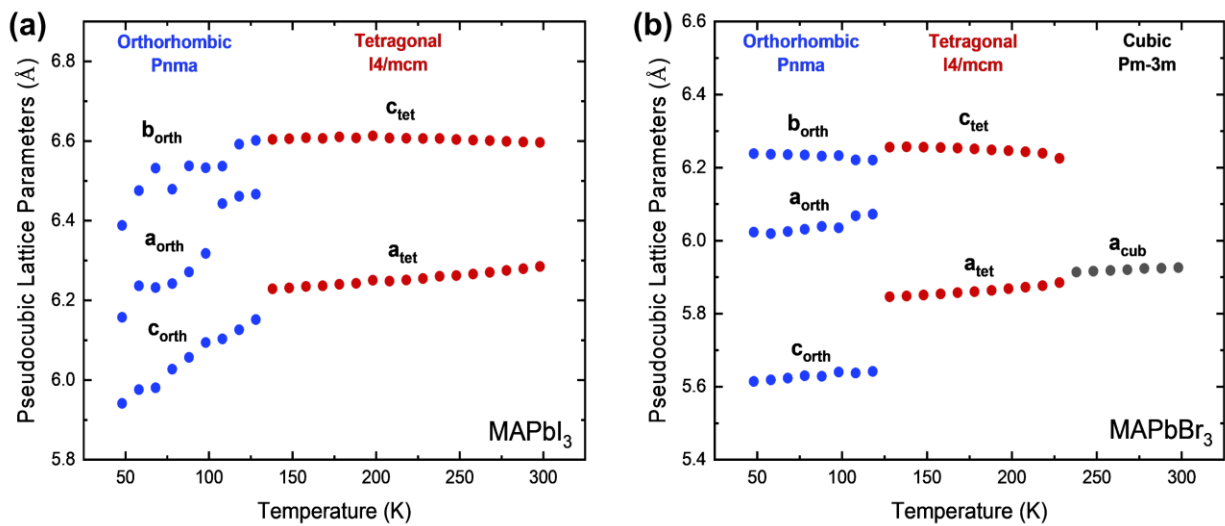


Figure S9. Lattice parameters of a) MAPbI₃ and b) MAPbBr₃ calculated from fitting to the PXRD patterns.

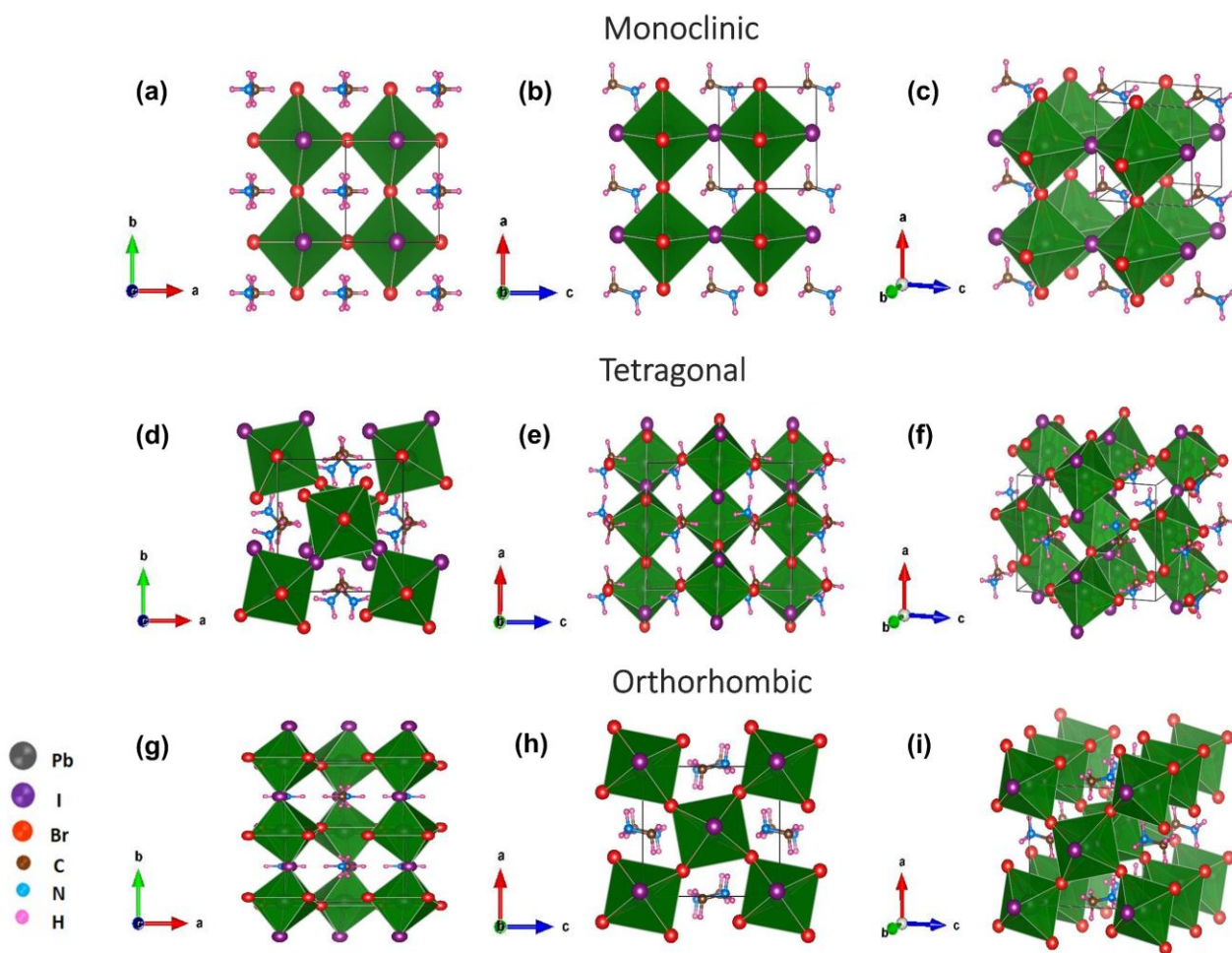


Figure S10. Crystal structures of MAPbI₂Br₂ in a-c) monoclinic, d-f) tetragonal, g-i) orthorhombic phases along c, b and rotated axis determined from DFT simulations. In the monoclinic phase, the octahedra are not rotated. The neighbouring planes of octahedra are rotated in the same (opposite) directions in orthorhombic *Pnma* (tetragonal *I4/mcm*) structures.

Section 3. Phonon Density of States Measurements

Table S2. Observed Phonon Modes from PELICAN with Both Configurations.

Sample	Detected phonon modes [meV]				
	Octahedral rotation		Coupled octahedral rotation and MA librations		MA torsion
MAPbI ₃	2.4	3.8	12	14.5	37
MAPbI ₂ Br	x	x	12	x	33.5
MAPbIBr ₂	x	x	11.6	x	33.5
MAPbBr ₃	3	5.5	11.8	x	36

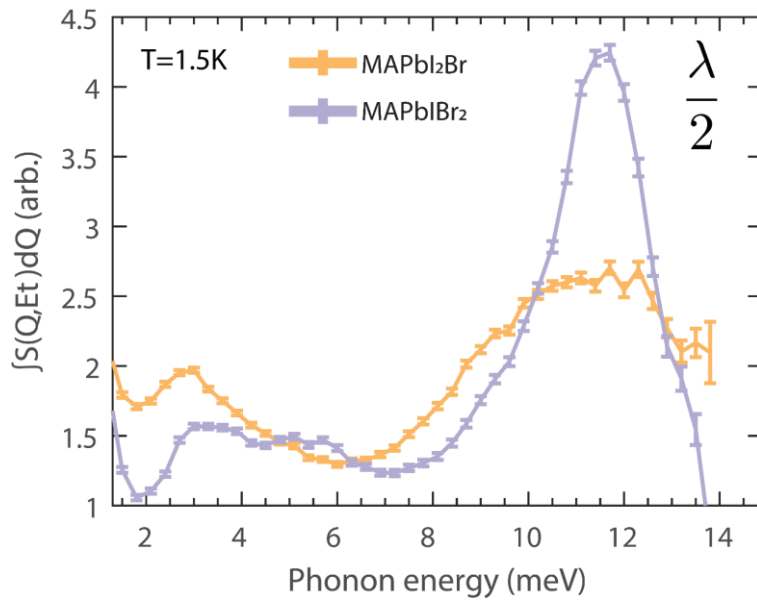


Figure S11. pDOS of MAPbI₂Br and MAPbIBr₂ measured at 1.5 K in $\lambda/2$ configuration with PELICAN. Error bars present confidence intervals of measured quantities.

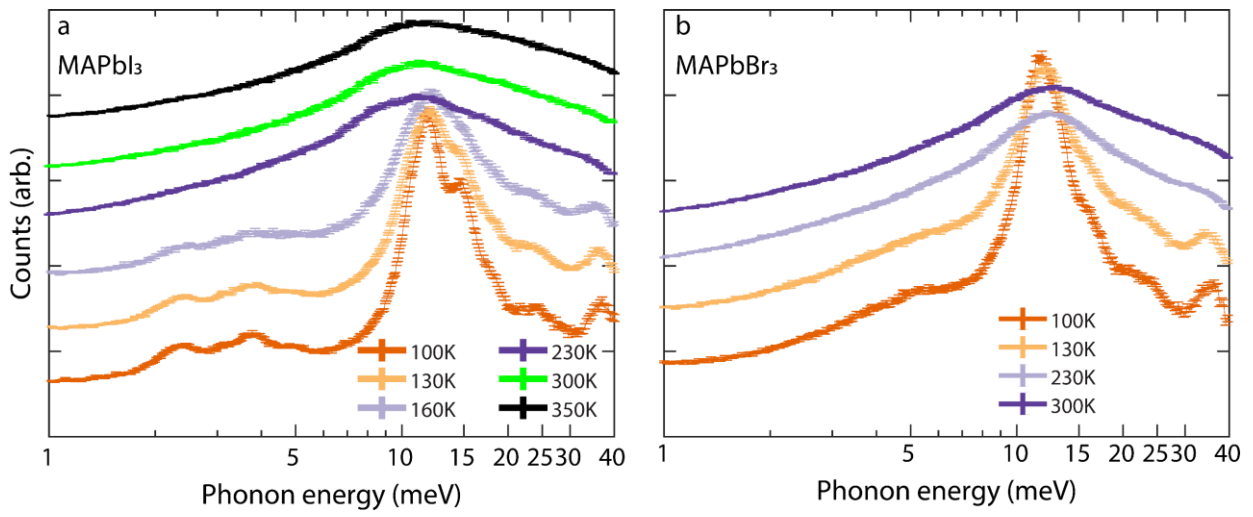


Figure S12. a) MAPbI₃, b) MAPbBr₃. Phonon melting observed between 160 K and 230 K region.

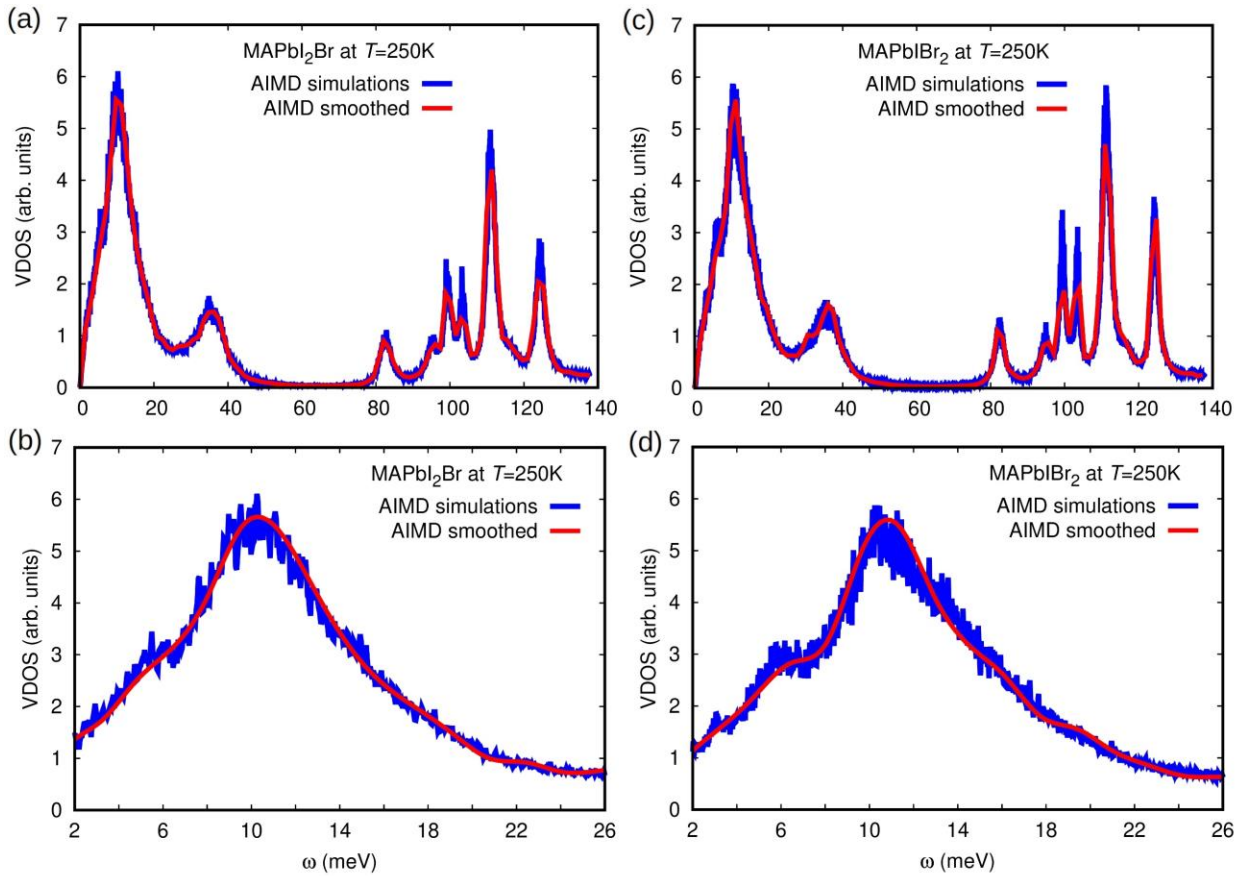


Figure S13. Vibrational density of states (VDOS) calculated for the mixed halides a,b) MAPbI₂Br, and c,d) MAPbIBr₂ at $T=250\text{K}$ from *ab initio* molecular dynamics (AIMD) simulations. The VDOS have been computed by performing the Fourier transform of the velocity auto-correlation function estimated over long simulation times of about $100\text{ ps}^{[5]}$. Subfigures a,c) show the VDOS estimated over a broad vibrational frequency range of 140 meV and subfigures b,d) show the VDOS estimated in the low vibrational frequency range $2 \leq \omega \leq 26\text{ meV}$.

Supplemental Methods

In the fitting of raw PXRD data, a direct derivation method with Pawley pattern decomposition method was applied, which can provide quantification results without correct atomic position information.^[6] The single-crystal XRD measurements were carried out on a Bruker D8 Quest Single Crystal diffractometer with a Photon II detector by using a I μ S 3.0 Microfocus source with Mo-K α radiation ($\lambda = 0.710723 \text{ \AA}$). The single crystal, mounted on the goniometer using cryo loops for intensity measurements, was coated with paraffin oil and then quickly transferred to an Oxford Cryo stream 800 attachment, which was set to the desired temperature during the experiment. Symmetry-related absorption corrections using the program SADABS^[7] were applied and the data were corrected for Lorentz and polarization effects using the Bruker APEX3 software.^[7] The structure was solved by ShelxT (intrinsic phasing),^[8] and the full-matrix least-square refinement was carried out using Shelxl^[8] in Olex2.

Supplemental References

- [1] Y. Nakamura, N. Shibayama, A. Hori, T. Matsushita, H. Segawa, T. Kondo, *Inorg. Chem.* **2020**, 59, 6709.
- [2] Y. Guo, O. Yaffe, D. W. Paley, A. N. Beecher, T. D. Hull, G. Szpak, J. S. Owen, L. E. Brus, M. A. Pimenta, *Phys. Rev. Mater.* **2017**, 1, 042401.
- [3] M. Simenas, S. Balciunas, J. N. Wilson, S. Svirskas, M. Kinka, A. Garbaras, V. Kalendra, A. Gagor, D. Szewczyk, A. Sieradzki, M. Maczka, V. Samulionis, A. Walsh, R. Grigalaitis, J. Banys, *Nat. Commun.* **2020**, 11, 5103.
- [4] D. Zhang, X. Hu, T. Chen, D. L. Abernathy, R. Kajimoto, M. Nakamura, M. Kofu, B. J. Foley, M. Yoon, J. J. Choi, S.-H. Lee, *Phys. Rev. B* **2020**, 102, 224310.
- [5] A. K. Sagotra, D. Chu, C. Cazorla, *Phys. Rev. Mater.* **2019**, 3, 035405.
- [6] H. Toraya, *J. Appl. Crystallogr.* **2016**, 49, 1508.
- [7] S. Bruker, S. J. M. SAINT, Wisconsin, USA, **2007**.
- [8] G. Sheldrick, *Acta Crystallogr. C* **2015**, 71, 3.